

Superconductivity induced by Ag intercalation in Dirac semimetal Bi_2Se_3

S. Koley^{1*} and Saurabh Basu²

¹ *Department of Physics, North Eastern Hill University, Shillong, Meghalaya, 793022 India and*

² *Department of Physics, Indian Institute of Technology Guwahati, Assam, 781039 India*

In this paper we have investigated the physical and transport properties of Bismuth Selenide, (Bi_2Se_3) intercalated with Silver (Ag) (Gold (Au) is included for comparison) via dynamical mean field theory with local density approximation. The band structure of Bi_2Se_3 with a Dirac cone is strongly influenced by the intercalation phenomena at moderate densities which eventually leads to an orbital selective metal insulator transition leading to superconductivity at low temperatures. The claims on the orbital selectivity are substantiated by computing the density of states. While the onset of superconducting correlations at low temperatures are supported by a sudden drop in the resistivity as a function of temperature and the nature of susceptibility. Further the Fermi surface (FS) maps for low and high temperature yields no FS reconstruction.

I. INTRODUCTION

Intercalation is a way of inserting a new material into a lattice without significantly changing its parent structure yet modifying its exotic physical and transport properties. In layered materials intercalation is a well known phenomenon and has good applications in a variety of materials, such as, battery electrodes, supercapacitors, and solid lubricants[1]. Recent studies have proved that intercalation in topological insulators can make the host material superconducting[2]. Search for these topological superconductors[3] is a new found interest of condensed matter physics. Topological insulators(TI) have insulating bulk states and topologically protected metallic surface states. These charge carriers are defined as the Dirac electrons where presence of finite spin-orbital coupling makes the spins of the electrons non-degenerate producing a spin-momentum locking effect.

The most renowned example of a 3D TI is Bi_2Se_3 , which has a Dirac cone on the surface and a large gap in the bulk [4]. The topological properties are addressed both theoretically and experimentally by ab initio electronic structure calculations[4] and electron scattering studies[5]. Bismuth selenide is a 3D layered chalcogenide having a narrow bandgap. Like other layered chalcogenides, it also exhibits diverse fascinating electronic properties. Presence of a van der Waals gap in the crystal structure makes it favorable for acting as a host for a number of intercalant materials, such as, Cu, Ag, Sr and many others [6]. Zerovalent intercalation[6] produces a variety of physical, electronic and magnetic properties, such as, Rb intercalation[7] that lead to strong Rashba spin-orbit coupling (SOC), while intercalating the host material with Sr and Cu make it superconducting [2, 8]. Further there are reported experiments also for controlling the positions of the Dirac points in Bi_2Se_3 by sur-

face doping[9]. Also incommensurate and commensurate charge density waves are reported in high density intercalation with copper in Bi_2Se_3 [10]. Thus intercalation introduces new features which do not exist in the host material. Moreover the intercalation process has renewed interest with the prospects of discovering new energy storage materials[11–14]. The alkali metals are used for doping surfaces of various topological materials for controlling the chemical activity of the surface. One of the most interesting features of the TI state is the valence and conduction bands of different parity cross and subsequently open up a band gap due to strong spin orbit interaction, thereby resulting in an inverted band structure leading to a Dirac semimetal regime. In Bi_2Se_3 Z_2 is the change in parity of the valence band eigenvalues at the band-inversion induced time-reversal-invariant point in the Brillouin zone.

With all the experimental and theoretical data cited above, it is needed to obtain information on the evolution of structural and electronic properties of the alkali atoms intercalated in Bi_2Se_3 . It is relevant to mention here that the intercalated compounds are stable; even large intercalant concentrations do not cause disruptions to the host lattice [6]. The parent Bi_2Se_3 , though can be argued as a weak coupling material, however some of the earlier experimental and theoretical studies support a strong correlation view[15]. Moreover defect induced Bi_2Se_3 also shows strong correlation due to the interacting $pp\sigma$ bond[16]. On the other hand, electron doped $\text{Cu}_x\text{Bi}_2\text{Se}_3$ shows an effective mass enhancement $m^*/m_e=2.6$ [17] where m_e is the free-electron mass. So for the bulk electronic states in intercalated Bi_2Se_3 strong coupling route is more appropriate in understanding the electronic and transport properties. Here we use first-principle density functional theory (DFT) calculations combined with dynamical mean field theory (DMFT) to show the intercalation induced changes in the electronic properties of Bi_2Se_3 with Ag and Au (Au is included for comparison) as intercalants. Here we have used 20% intercalation for Ag throughout this work. Earlier experimental studies [6] show Ag intercalation, with concentration greater than 50% exhibits

* sudiptakoley20@gmail.com; Present Address: Department of Physics, Amity Institute of Applied Sciences, Amity University, Kolkata, 700135, India

strong satellite peaks associated with a host Bragg red peak which are recognized as a signature of an incommensurate charge density wave[18] in superlattice intercalate systems. The positions of the peaks suggest of a change in the natural periodicity of the Ag intercalated Bi_2Se_3 . While Ag intercalation affects the periodicity of the material, experiments suggest that Au intercalation only results in crystal defects. Here we shall show how they affect the Dirac points and the transport properties of the parent Bi_2Se_3 .

The rest of the paper is structured as follows. A brief description of the method, that is, DFT plus DMFT, alongwith the Hamiltonian are outlined in section II. The results and discussions appear in section III. Hence we conclude with a summary of our main results in section IV.

II. DFT PLUS DMFT

Bi_2Se_3 has a rhombohedral structure (space group: $R\bar{3}m$). The crystal structure consists of quintuple layered blocks separated by a van der Waals gap, and in each layer, the hexagonal atomic planes are arranged following the sequence of Se1-Bi-Se2-Bi-Se1 along the z -direction with covalent bonding between the atoms. Se1 and Se2 are two inequivalent Selenium atoms. Thus any of the quintuple layers ends or starts with a Se1 atom and any foreign atom placed in the van der Waals gap will be closer to the Selenium atom. We add further comments on the structure and its stability in the supplementary information.

First principles calculations were performed using WIEN2k full-potential linearized augmented plane wave (FP-LAPW) ab initio package[19] within the DFT formalism[20] to get the electronic structure and density of states (DOS). A $10 \times 10 \times 10$ k -mesh (with the cutoff parameter, $Rk_{max} = 7.5$) is employed here and a generalized gradient approximation Perdew-Burke-Ernzerhof (GGA-PBE) exchange correlation potential is chosen. The muffin-tin radius, R_{mt} is chosen to be 2.5 a.u. for Bi, Se, Au and Ag for different intercalation densities. The cell parameters and the (fractional) atomic coordinates are derived following earlier experiment[6], and then these parameters are varied to get the energy minimized crystal structure in the intercalated Bi_2Se_3 . Finally the self consistent field (scf) calculations are computed with an accuracy of 0.0001 eV. Thus from the converged scf calculations we have figured out the band structure and the DOS. The band structure and atom-resolved DOS is displayed in Fig.1 and Fig.2. The DOS manifests partially occupied Se-4p, Bi-6p and Ag-5s bands (denoted later as a, b, c orbitals respectively) near the Fermi level in Ag intercalation, whereas Se-4p, Bi-6p and Au-6s (denoted later as a, b, c orbitals respectively) bands near the Fermi level in the Au intercalated Bi_2Se_3 . Our results for the parent Bi_2Se_3 are in accordance with the previous calculations[21]. For example, the energy bandgap

of about 0.3 eV which matches nicely with the earlier experimental data. We have calculated the parent bandstructure both with and without the spin-orbit coupling (SOC). Comparing both of them with the existing results, we have concluded that SOC induces an anti-crossing feature around the Γ point which indicates inversion of the conduction and the valance band, thereby showing Dirac semi-metallic nature of Bi_2Se_3 .

For performing electronic and transport calculations, a fully charge-self-consistent dynamical mean field theory (DMFT) is used. In a strongly correlated system, DFT *plus* DMFT has been successful in explaining a lot of important physics [22, 23]. The multi-orbital iterated perturbation theory (MO-IPT), a computationally fast and effective impurity solver has been used here. Though not exact, it works nicely in real systems at both high and low temperature regimes[24]. MO-IPT is an approximate method that relies on an interpolation from the second order perturbation theory for the impurity problem. The interpolation preserves the correct high frequency limit for the self-energy and is exact in both the non-interacting and the atomic limits. To present the importance of quantum correlations in an intercalated Bi_2Se_3 we have used multi-orbital Hubbard model with reasonable values for the intra and inter-orbital Coulomb interactions. The total Hamiltonian is expressed as,

$$H = \sum_{k,a,b,\sigma} (\epsilon_{k,ab} + \mu_a \delta_{ab}) c_{k,a,\sigma}^\dagger c_{k,b,\sigma} + U \sum_{i,a} n_{i a \uparrow} n_{i a \downarrow} + U' \sum_{i,a,b,\sigma,\sigma'} n_{i a \sigma} n_{i b \sigma'} - J_H \sum_{i,a,b} S_{i a} \cdot S_{i b} \quad (1)$$

where $\epsilon_{k,ab}$ stands for the intra and inter-orbital hopping between three bands which are the hybridization of the p-orbitals of Bi, Se and the s orbital of Ag (or Au) that include the effect of SOC also and $U' = U - 2J_H$ where U and U' are the intra- and inter-orbital Coulomb repulsion parameters and J_H is the Hund's coupling. Here we have considered $J_H = 0.5$ eV and varied U over a range, namely $0.5 \text{ eV} \leq U \leq 3.5$ eV (Fig.3).

III. RESULTS AND DISCUSSION

We shall begin discussing our DFT *plus* DMFT results. In Fig.3 we present the orbital resolved spectral functions of the intercalated Bi_2Se_3 as a function of the on-site Coulomb repulsion, U . Intercalation increases the density of conduction electrons at the Fermi level. As observed from the DMFT density of states, with increasing U , there is large spectral weight transfer in both cases of intercalation with Ag (Fig. 1c) and Au (Fig. 1d). The spectral weight transfer as a function of the Coulomb interaction and the low energy quasiparticle resonance are intrinsic to strongly correlated systems. The emergence of the Hubbard bands with increasing U is also

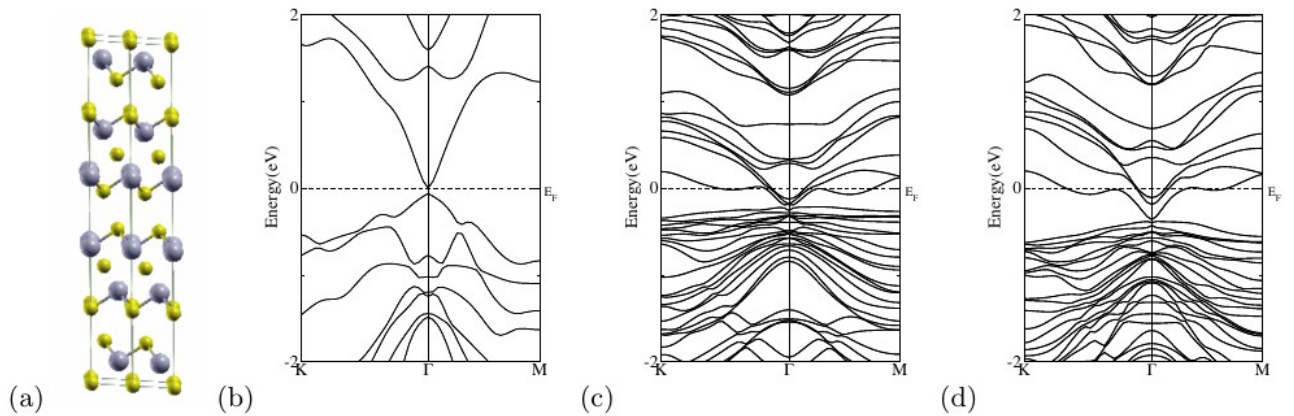


FIG. 1. (Color Online) (a) The crystal structure of Bi_2Se_3 . Band structure of (b) parent Bi_2Se_3 , (c) Ag intercalation and (d) Au intercalation in the rhombohedral structure including spin-orbit coupling (SOC). Intercalation results in disappearance of the band inversion at the Γ point and results in increase in the number of conduction electrons. For the effective three-band model incorporating conduction electrons within DMFT calculations, we use the Bi-p, Se-p and Ag-5s or Au-6s bands crossing Fermi Energy ($E_F=0$) for DMFT calculation.

noteworthy in the intercalated Bi_2Se_3 . For the Au intercalated system, the electron-electron interaction only transfers the spectral weight and the material remains a correlated metal for all values of U , whereas for the Ag intercalation, increasing U introduces selective gaps in the orbital density of states which is most prominently seen for $U = 3.0$ eV. In this case, the large U limit distorts the low energy coherence and a selective Mott-Hubbard gap opens up, thereby promoting the formation of experimentally reported charge density wave (CDW) state with a different periodicity. Thus existence of an orbital selective Mott scenario in the Ag intercalated Bi_2Se_3 in the normal state is related to the strong scattering which might induce CDW order with increasing temperature.

Several interesting features emerge from our results, such as, the correlated electronic structure and the orbital dependent spectral weight redistribution depending on the strengths U and U' . The incoherent Hubbard bands are prominent at higher energies as observed in the strongly correlated system. While earlier theoretical results[15] for the parent compound, Bi_2Se_3 have reported a Kondo-Mott electronic transition in the bulk system induced by dynamical correlations and active in all the orbitals, here we get an orbital selective Mott transition in the Ag intercalated compound.

With this orbital selective DOS in Fig.3a (choosing $U = 3.0$ eV and $U' = 2.0$ eV), we demonstrate how electron correlations are affected with the inclusion of thermal effects. In Fig.3c and Fig.3d we show the temperature dependence of Ag and Au intercalated DOS re-

spectively. It is observed that Ag band exhibits a peak at the Fermi energy at all values of temperature, while there is a pseudogap increasing in the Se-p band with decreasing temperature, although the Bi-p band remains almost unaffected. These contrasting behaviors are outcomes of multi-orbital electronic correlations on non-interacting DOS. While at lower temperatures, the Se-p band remains insulating, but the Bi-p and the Ag-s bands retain their metallic nature, thereby revealing an interesting physics in these systems.

Such a scenario can open the possibility of giving rise to novel instabilities with competing orders, as those observed in doped TiSe_2 [27]. Interestingly, at $T = 100\text{K}$ the orbital selectivity vanishes and a sharp peak appears at the Fermi level from below. Whereas earlier x-ray diffraction data[6] show that there is formation of a CDW order in the intercalated compound, here we find opening of a pseudogap below 100K. This is a novel finding in these types of systems.

Further we have computed the optical conductivity in Fig.4 as a function of energy for a few different values of temperature, T from the DMFT Green's function. The DMFT equation for optical conductivity is as follows,

$$\sigma(\omega) = \sigma_0 \int d\epsilon \rho_0(\epsilon) \int d\nu \frac{f(\omega + \nu) - f(\nu)}{\omega} \rho_\epsilon(\omega + \nu) \rho_\epsilon(\nu)$$

where the density of states, $\rho_\epsilon(\omega)$ is defined as, $\rho_\epsilon(\omega) = \sum_{a=1}^2 \rho_{\epsilon_a}(\omega) = (-1/\pi) \sum_{a=1}^2 \text{Im}[1/(\omega + \mu_a - \epsilon_a - \Sigma_a(\omega))]$, and $f(\nu)$ is the Fermi function. In DMFT, the above calculation for optical conductivity is simplified and the

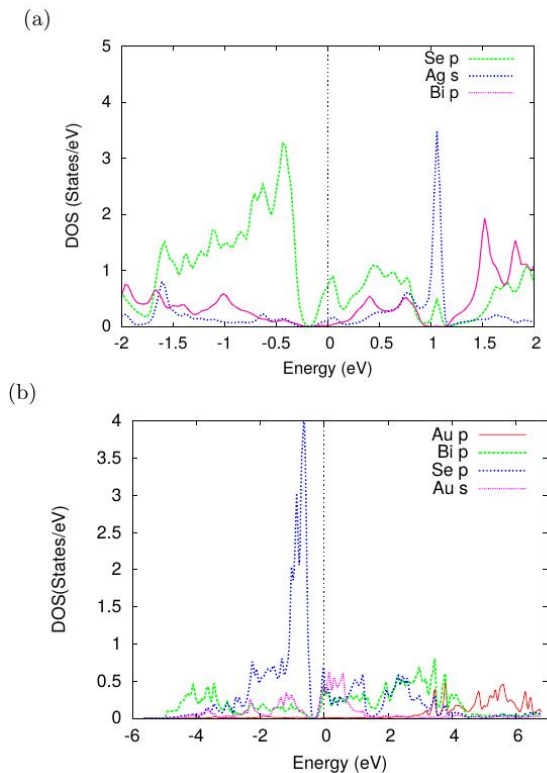


FIG. 2. (Color Online) Density of states of the (a) Bi-p, Se-p and Ag-5s and (b) Bi-p, Se-p and Au-6s orbitals from DFT calculation.

transport coefficients can be computed directly from the DMFT propagators[25]. The simplifications originate from the fact that the irreducible vertex corrections vanish for a one-band case and turn out to be surprisingly small corresponding to a multiband case. In the optical conductivity corresponding to both the systems we have plotted the relevant energy range from the band structure for those three bands which are crossing Fermi level. In Ag intercalation, specifically up to an energy of about 0.5 eV, the optical conductivity lineshapes show sizable spectral weight transfer with increasing temperature. The sharp peak in the conductivity at low temperature is not a Fermi Liquid (FL) Drude peak, rather this peak arises due to reduced incoherence induced by the CDW transition. Clear spectral weight transfer upto 1 eV is discernible from the conductivity lineshapes, which is a very high value in comparison with the energy range for the bands indicating large dynamical correlations. The overall change in the optical conductivity points towards appearance of an order. In contrast, Au intercalation shows a FL ($\text{Im}\Sigma(\omega) \simeq 0$ as $\omega \simeq 0$ where $\Sigma(\omega)$ is DMFT self energy) behavior (consistent with the DOS data from our DMFT calculations) throughout the temperature range. It shows a featureless broad peak till about 0.53 eV and an additional Drude peak at lower energies. The low en-

ergy peak height decreases with temperature, and along with a spectral weight transfer occurs at higher energies.

We next compute the dc resistivity from our dynamical mean field theory. The analysis of our resistivity data (inset of Fig.4a) shows linear in T behavior of the Ag intercalated compound over a large range of temperature, and all the way till room temperature. This is one of the key results of our paper which allows us to conclude that the transition to an ordered phase is a coherence restoring transition which occurs at higher temperatures. The linear T dependence of resistivity is in good accord with the finding of a CDW order in experiments, and hence mandates deeper microscopic exploration. However for the Au intercalation, there is no such orbital selectivity and the spectral function drastically changes at temperatures greater than 10K. All the three bands continue to show metallic behavior throughout the temperature range. Clearly the case concerning the intercalation of Au differs significantly from that of Ag.

Let us look at the low temperature scenario. To show the behavior of $\rho(T)$ at lower temperatures, we have plotted it separately in the lower inset of Fig.4a in the range 0-10K which shows sharp decrease in resistivity (nearly vanishing) occurring between 2K and 5K. This provides a theoretical evidence of finding superconductivity in the Ag intercalated Bi_2Se_3 . The inset of Fig.4b shows the temperature dependent resistivity of Au intercalated Bi_2Se_3 . Consistent with findings of the FL behavior, the dc resistivity shows T^2 dependence throughout the temperature range. Thus, as predicted from experiments, Au intercalation only introduces defects in the Bi_2Se_3 crystal lattice which makes the system metallic.

Although Ag is plasmonic, however onset of superconductivity with doping by Ag is not new phenomena. It was reported earlier that an enhancement of T_c can be achieved with Ag present in a semiconductor matrix[26].

Now to explore the microscopic origin of ordering in Ag intercalated Bi_2Se_3 , we compute DMFT Fermi surface (FS) (Fig.5) at high and low temperature. In parent Bi_2Se_3 due to band inversion, there is no Fermi level crossing, thus resulting in no pockets in the FS map. Strong spin-orbit interaction eliminates the possibility of FS nesting. From the DMFT Fermi surface estimations, the presence of selective gaps is observed, though there is no Fermi surface reconstruction with temperature, which is in accordance with the corresponding features realized for iron superconductors and chalcogenides and the superconductivity is originated due to electron electron interaction [27]. The two particle interaction, obtained to second order is proportional to ϵ_{ab}^2 , which is more relevant in ordered low T region. The interaction is $H_{res} \simeq -\epsilon_{ab}^2 \chi_{ab}(0,0) \sum_{\langle i,j \rangle, \sigma\sigma'} c_{ia\sigma}^\dagger c_{jb\sigma} c_{jb\sigma'}^\dagger c_{ia\sigma'}$, with $\chi_{ab}(0,0)$ the inter-orbital susceptibility calculated from the normal state DMFT results. Now the new effective Hamiltonian is $H = H_n + H_{res}^{HF}$, where $H_n = \sum_{k,\nu} (\epsilon_{k,\nu} + \Sigma_\nu(\omega) - E_\nu) c_{k,\nu}^\dagger c_{k,\nu} + \sum_{a \neq b, (k)} \epsilon_{ab} (c_{k,a}^\dagger c_{k,b} + h.c.)$, with $\nu = a, b$. The residual Hamiltonian H_{res}^{HF} is found

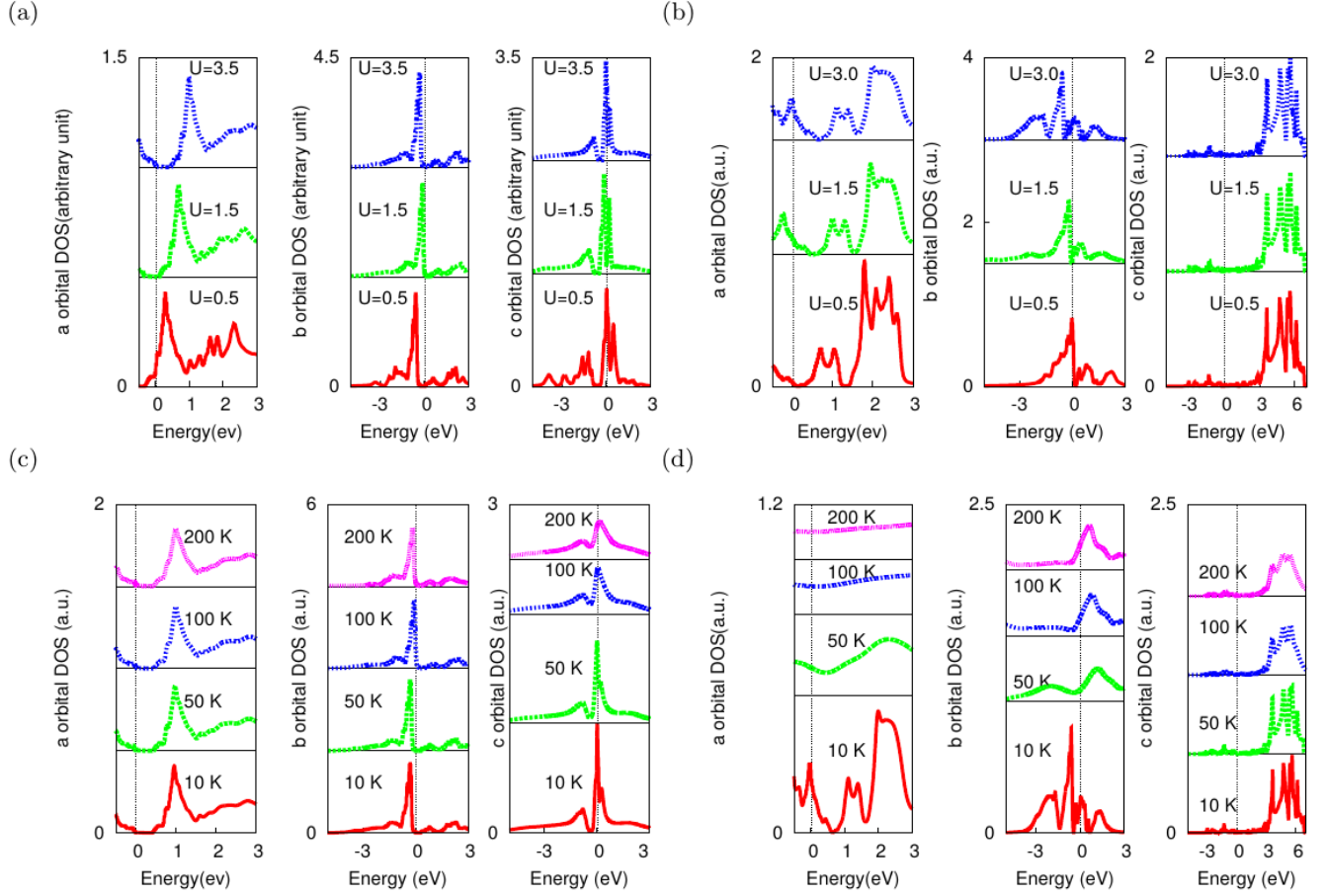


FIG. 3. (Color Online) Orbital-dependent density of states from DFT+DMFT at various values of U for (a) Ag intercalation and (b) Au intercalation. DFT+DMFT density of states at various temperatures for both Ag and Au intercalations respectively ((c) and (d)). Density of states are shifted in the y -axis to reflect changes induced by coulomb interaction ((a) and (b)) and due to the inclusion of temperature ((c) and (d)). different colors are used for different U and T .

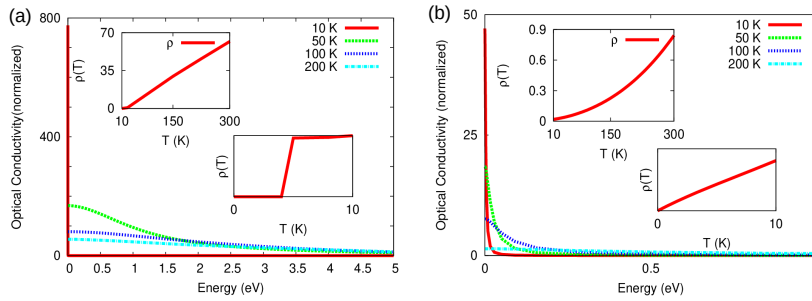


FIG. 4. (Color Online) Optical conductivity (normalized with respect to normal state value) of (a) Ag and (b) Au intercalated Bi_2Se_3 . For Ag intercalation, high temperature optical conductivities (50 K-200K) are multiplied by 1000 to show their variation in comparison with 10 K since the corresponding values are very small. Inset shows resistivity plot at two different temperature range, namely, 10K-100K and 0K-10K. For Ag intercalation, the resistivity at low temperature range shows sudden decrease below 5K.

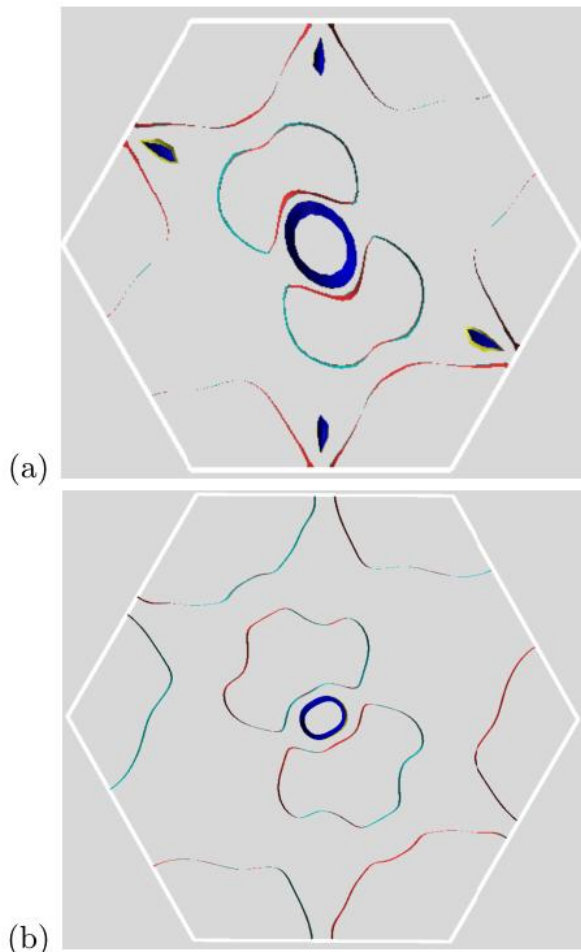


FIG. 5. (Color Online) DMFT Fermi surface map for Ag intercalated Bi_2Se_3 at (i) low (10K) and (ii) high(200 K) temperature. The central pocket changes its lineshape along with disappearance of pockets at the M points.

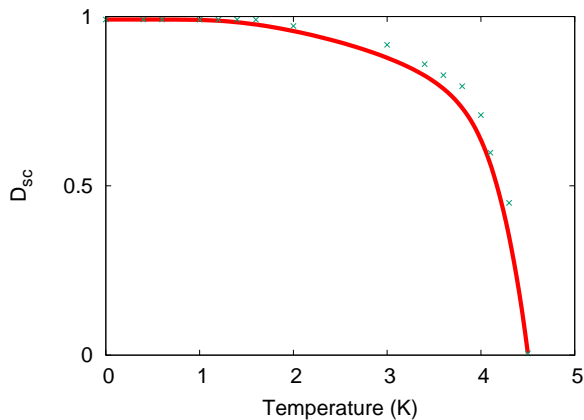


FIG. 6. (Color Online) DMFT superconducting order parameter plot with temperature. Red line is a fit to the actual data points which are represented by green points.

by decoupling the intersite interaction in a generalised Hartree Fock(HF) sense. Now this will produce ordering in particle-particle (SC) channel. The HF Hamiltonian is $H_{res}^{HF} = -p \sum_{\langle i,j \rangle, a,b,\sigma,\sigma'} (\langle n_{i,a} \rangle n_{j,b} + \langle n_{j,b} \rangle n_{i,a} - \langle c_{i,a,\sigma}^\dagger c_{j,b,\sigma'}^\dagger \rangle c_{j,b,\sigma'} c_{i,a,\sigma} + h.c.)$ (where p is proportionality constant). We studied here the superconducting phase with the two particle instability in particle-particle channel (with parametrized $p=0.1$) and the superconducting order parameter can be calculated from $D_{sc} \propto \langle c_{i,a,\sigma}^\dagger c_{j,b,\sigma'}^\dagger \rangle$ which yields multiband spin-singlet SC. The anomalous Green's function: $F(k, \tau) \equiv -\langle T_\tau c_{k\uparrow}(\tau) c_{-k\downarrow}(0) \rangle$ satisfying $F(-k, -\tau) = F(k, \tau)$ for s wave pairing is introduced in the low temperature phase of intercalated Bi_2Se_3 . We presented superconducting order parameter calculated self consistently from DMFT in Fig.6. The order parameter follows $(1 - T/T_c)^{0.5}$ behaviour and vanishes at 4.5 K where the resistivity also drops.

The electron-electron interaction induced ordering is supported by negligible temperature effects on the Fermi surface lineshapes. Now in the Ag intercalation case, high temperature orbital selectivity is observed which affects the FS too. The high temperature FS is substantially smeared out at the M points. Further examination of the DMFT FS map at the Γ point reveals that the central pocket acquires an oblong shape, instead of being hexagonal, as is usually expected from the DFT results. This change in FS can possibly arise due to the orbital dependent reconstruction as a result of the inter-orbital interactions. Further at low temperatures, the electron pockets near the Γ point change their shape. New FS sheets appear at low temperatures at the M point. Since these features become well defined at low temperature, that is at temperatures below which superconductivity is predicted, it should be a direct consequence of superconducting order induced reconstruction of electronic states.

IV. CONCLUSIONS

To summarize, here we have presented a DFT *plus* DMFT study of Ag and Au intercalated Bi_2Se_3 to explore the ordering induced by these intercalants. The work is focused mainly on the changes in electronic and transport properties that occur in this scenario from our DFT calculations. The electronic band structure of parent Bi_2Se_3 displays signature of a Dirac semimetal, which substantially changes due to intercalation. Intercalation with Ag induces an increase in the conduction electron density and the band inversion at the Γ point disappears. We have also observed an orbital selective Mott-Hubbard gap and studied effects of the interaction parameter therein. Interestingly at low temperature, superconducting correlations emerge that are convincingly shown by a sudden drop in the resistivity below $T_c \sim 4.5\text{K}$ which is further supported by the plot of superconducting order param-

eter which drops to zero at T_c . Finally the absence of a structural transition induced is confirmed by the FS maps at both low and high temperature. The latter suggests that the FS is gapped only in certain directions and hence invalidates the concept of nesting as the origin of order. Armed with all the DMFT results, including the resistivity data with an effective three-band model, the onset of superconductivity is predicted with Ag intercalation. This study can be used to other layered materials with similar structure like other layer topological compounds emerging as a novel research topic for its application in energy storage.

Acknowledgement S. Koley acknowledges DST women scientist grant SR/WOS-A/PM-80/2016(G) for finance and also thank Prof. M C Mahato for mentoring and useful conversations. SB acknowledges financial support from the SERB grant No. EMR/2015/001039.

-
- [1] T. Wang et al., *Adv Sci* **4**, 1600289 (2017).
- [2] G. Du et al., *Nature Communications* **8**, 14466 (2017).
- [3] M. Sato and Y. Ando, *Rep. Prog. Phys.* **80**, 076501 (2017).
- [4] H. Zhang et al., *Nature Physics* **5**, 438 (2009).
- [5] J. A. Sobota et al., *J. Electron Spectrosc. Relat. Phenom.* **195**, 249 (2014).
- [6] K. J. Koski et al., *J. Am. Chem. Soc.* **134**, 13773 (2012).
- [7] M. Bianchi et al., *ACS Nano* **6**, 7009 (2012).
- [8] Y. S. Hor et al., *Phys. Rev. Lett.* **104**, 057001 (2010).
- [9] T. Valla et al., *Phys. Rev. Lett.* **108**, 117601 (2012).
- [10] K. J. Koski et al., *J. Am. Chem. Soc.* **134**, 7584 (2012).
- [11] W. Müller-Warmuth, and R. Schöllhorn (Eds.) *Progress in Intercalation Research*, Kluwer: Dordrecht, The Netherlands, (1994); M. S. Dresselhaus, *Intercalation in Layered Materials*; NATOASI Series, Subseries B, Physics, Vol. 148; Plenum Press: New York, (1987); F. Levy *Intercalated Layered Materials* Reidel: Dordrecht, The Netherlands, (1979); M. S. Whittingham and A. J. Jacobson (Eds.) *Intercalation Chemistry* Academic Press: New York, (1982).
- [12] A.S. Aricò, P. Bruce, B. Scrosati, J.M. Tarascon, and W. V. Schalkwijk, *Nat. Mater.* **4**, 366 (2005).
- [13] M.S. Whittingham *J. Solid State Chem.* **29**, 303 (1979).
- [14] K. Kang. et al., *Science* **311**, 977 (2006); J.M. Tarascon and M. Armand *Nature* **451**, 652 (2008).
- [15] L. Craco, *Eur. Phys. J. B* **88**, 292 (2015); L. Craco and S. Leoni *Phys. Rev. B* **85**, 075114 (2012).
- [16] S. Urazhdin, D. Bilc, S.H. Tessmer, S.D. Mahanti, *Phys. Rev. B* **66**, 161306(R) (2002).
- [17] M. Kriener, K. Segawa, Z. Ren, S. Sasaki, and Y. Ando, *Phys. Rev. Lett.* **106**, 127004 (2011).
- [18] J. A. Wilson, F. J. Di Salvo and S. Mahajan, *Adv. Phys.* **24**, 117 (1975).
- [19] P. Blaha, K. Schwarz, G.K.H. Madsen, D. Kvasnicka, and J. Luitz, *WIEN2k, An Augmented Plane Wave + Local Orbitals Program for Calculating Crystal Properties* (Wien:Karlheinz Schwarz, Techn. Universität Wien, 2001).
- [20] T.L. Loucks, *Augmented Plane Wave Method* (New York:Benjamin, 1967); O.K. Andersen, *Solid State Commun.* **13**, 133 (1973); E. Wimmer, H. Krakauer, M. Weinert, and A.J. Freeman, *Phys. Rev. B* **24**, 864 (1981).
- [21] S. K. Mishra, S. Satpathy, and O. Jepsen, *J. Phys. Condens. Matter* **9**, 461 (1997); P. Larson *Phys. Rev. B* **74** 205113 (2006).
- [22] A. Taraphder, S. Koley, N.S. Vidhyadhiraja, and M.S. Laad, *Physical Review Letters*, **106**, 236405 (2011).
- [23] S. Koley, M.S. Laad, N.S. Vidhyadhiraja, and A. Taraphder, *Physical Review B*, **90**, 115146 (2014).
- [24] A. Georges et al., *Rev. Mod. Phys.* **68**, 13 (1996).
- [25] J M. Tomczak and S. Biermann, *Phys. Rev. B* **80**, 085117 (2009).
- [26] D. Djurek, arXiv:0905.3524 (2009); D. Djurek, arXiv:0811.4352 (2009)
- [27] S. Koley, *Solid State Communications* **251**, 23 (2017); S. Koley, arXiv:1808.02298 (2018).